NWRI CONTRIBUTION 85-139

Beltaos (35)

INITIAL FRACTURE PATTERNS OF RIVER ICE COVER

by

S. Beltaos

Environmental Hydraulics Section
Hydraulics Division
National Water Research Institute
867 Lakeshore Road, P.O. Box 5050
Burlington, Ontario L7R 4A6

November 1985

MANAGEMENT PERSPECTIVE

Ice cover failure at spring breakup is governed by thermodynamic and physical laws. In principle therefore, it is possible to describe the initial breakup process. This paper describes possible mechanism, backed up by observation, for the breakup process and the subsequent form of the loose ice cover.

The analysis brings order and insight to the early stages of breakup which is an essential first step to logical forecasting and management of rivers subject to spring ice jams.

T. Milne Dick
Chief
Hydraulics Division

PERSPECTIVE-GESTION

La rupture de la couche de glace durant le dégel du printemps est régie par les principes de la thermodynamique et de la physique. Il est donc possible de décrire, en théorie, le processus initial d'une débâcle. Ce document présente une description, fondée sur des observations, du mécanisme de rupture des glaces et du comportement subséquent des plaques de glace détachées.

Cette analyse explique le déroulement des phases initiales du phénomène de la débâcle, étape importante du processus de prévision logique et de la gestion des embâcles printaniers dans les cours d'eau.

Le chef,

T. Milne Dick
Division de l'hydraulique

ABSTRACT

River ice breakup is often attended by destructive ice jams. While considerable progress has been made in predicting features of jams once they have formed, little is known about the processes by which an intact ice cover is fractured during the early phases of the breakup period. Understanding these processes would be of benefit to forecasting the onset and severity of breakup.

Two frequently observed types of early fracture are longitudinal and transverse cracks. When runoff begins, uplift pressures develop on the underside of the shore fast ice cover. Analysis, based on the theory of beams supported by elastic foundations, shows that longitudinal cracks are likely to develop soon after the flow begins to increase. For usual stream sizes and ice conditions, two cracks (sometimes called "hinge" cracks) are predicted, thus subdividing the ice cover into a main, central part and two side-strips. Where ice thickness is very large or the channel width too small, a single mid-channel crack is predicted. Field observations support the theory.

With continued increase in discharge, the central portion of the ice cover may eventually detach from the side strips and thus become subject to transverse fracture. Transverse cracks may form by bending on vertical or horizontal planes. Vertical bending may arise from the deformed shape of the water surface owing to unsteady flow. It is shown that fracture of this type requires extreme water surface slopes, unlikely to result from runoff processes alone but possibly occurring briefly during surges from released ice jams.

Horizontal bending results primarily from flow shear and the meandering planform of natural streams. Fracture by horizontal bending does not require surge action and could account for transverse crack patterns observed in the Thames River (Ontario).

RÉSUMÉ

La rupture de la couche de glace sur les cours d'eau est souvent suivie d'embâcles destructeurs. Même si des progrès considérables ont été réalisés dans les méthodes de prévision du comportement des embâcles après leur formation, on possède peu de détails sur les premières phases du processus de rupture d'une couche de glace intacte. Il serait utile d'en savoir plus long sur le sujet, de façon à être en mesure de prévoir le déclenchement et la gravité des embâcles.

On a remarqué qu'il se produisait tout d'abord des fissures longitudinales et transversales. Lorsque le ruissellement débute, des sous-pressions sont créées à la surface interne de la couche de glace solide près du rivage. Les analyses, fondées sur la théorie des poutres soutenues par une base élastique, démontrent que des fractures longitudinales semblent apparaître dès que le courant commence à s'intensifier. Pour des cours d'eau moyens et dans des conditions normales de glace, on prévoit que deux fractures (quelquefois appelées fractures "charnières") se formeront, divisant ainsi la couche de glace en une plaque centrale principale avec deux bandes latérales. On pense que si la couche de glace est très épaisse ou si le canal est étroit, une seule fracture apparaîtra. Cette théorie est appuyée par des observations sur le terrain.

Si le débit continue d'augmenter, la plaque centrale de la couche de glace pourra éventuellement se détacher des bandes latérales et à son tour, sera peut-être divisée par des fractures transversales. Ces fractures transversales peuvent être produites par des courbures des plans vertical et horizontal. La déformation de la surface de l'eau causée par l'irrégularité des courants peut produire une courbure verticale de la glace. Il a été démontré que ce phénomène ne se produira que si la pente de la surface de l'eau est très prononcée, condition ne résultant vraisemblablement pas du ruissellement seul, mais plutôt du déferlement des glaces à la suite de la dislocation d'un embâcle.

Les courbures horizontales sont principalement causées par l'action des crêtes de courant et la forme en plan sinueuse des cours d'eau naturels. La surpression n'est pas nécessaire à la formation du fractionnement causé par des courbures horizontales; ce fractionnement pourrait expliquer le plan des fractures transversales observé dans la rivière Thames (Ontario).

1.0 INTRODUCTION

The breakup of river ice is a brief but important period of the year because of the frequent formation of destructive ice jams. While considerable progress has been made in predicting features of ice jams after they have formed, little is known about the processes by which a continuous ice cover is broken into the small fragments that comprise an ice jam. Understanding these processes would be of benefit to forecasting both the onset and the severity of river ice breakup.

Two common occurrences of the initial phases of breakup are investigated herein, namely the formation of longitudinal and transverse cracks. In this manner, the initially continuous ice cover is broken down into separate ice sheets which often sets the stage for breakup "initiation", if this event is defined as the time when the ice cover is set in motion. Once this occurs, further fragmentation is rapid, owing to impacts of moving ice sheets either on channel boundaries or on other sheets. Clearly, the initial pattern of fracture governs the sizes of separate ice sheets which in turn may have an effect on the conditions for breakup initiation and, later on, on the location and persistence of ice jams.

2.0 LONGITUDINAL CRACKS

2.1 Physical Considerations and Assumptions

Consider the case of an ice-covered river reach, in which steady unifom flow prevails, as is approximately the case during the winter period. The flow under the cover can be described as gravity-driven with nearly hydrostatic pressure distribution.

When warm weather and increased runoff start, the discharge will begin to increase with time and upstream distance. So long as the cover remains integral and attached to the river banks, a pressure gradient must develop to accommodate the increased discharge. The

flow will thus become of the conduit type and be partly pressure-driven. Increasing uplift pressures will be applied to the ice cover until the latter's strength is exceeded and cracks form. Once this occurs, the water will be free to assume a higher stage and revert to purely gravity-driven flow while the cracked cover will float to a higher position.

Prior to crack formation, the structural situation is that of a floating ice plate, supported at the edges and subjected to a distributed load, p, as illustrated in Fig. 1. Considering the total upward pressure, p_T, applied on the underside of the ice cover at its deformed state, we obtain:

$$p_T = p + \gamma(s_i h_i - w) - \gamma_i h_i \qquad (1)$$

in which γ, γ_i = unit weights of water and ice, respectively; h_i = ice cover thickness; w = deflection of the ice cover; and s_i = γ_i/γ = specific gravity of ice ≈ 0.92. Eq. 1 can be simplified to

$$p_T = p - \gamma w \qquad (2)$$

which suggests that the ice cover may be viewed as a plate subjected to an upward distributed load, p, and supported by an elastic foundation* of modulus γ. Eqs. 1 and 2 are valid so long as the bottom of the ice cover does not emerge above the water level, i.e., $w \leq s_i h_i$. This condition is usually satisfied in practice and will be assumed to apply herein. The load p is laterally uniform but must vary with longitudinal distance and time in view of the unsteady flow conditions that prevail when the discharge starts to increase. The actual situation is thus too complex for analytical solution but can

---

* An elastic foundation produces a reaction that is proportional to the local deflection. The coefficient of proportionality is termed the foundation modulus.

be considerably simplified by making the following two assumptions: (a) dynamic effects are negligible; and (b) the longitudinal gradient of p is small. These assumptions can be verified by an order-of-magnitude analysis (see Appendix A). The solution can thus be based on the theory of beams resting on elastic foundations (Hetenyi 1946). A solution for infinitely long beams (very wide channel) has been obtained by Billfalk (1981).

2.2 Analytical Relationships

For a beam of arbitrary length, Hetenyi (1946) gives the following expressions for the bending moment:

$$\frac{2\lambda^2 M}{p} = \frac{\sinh\lambda z \sin\lambda z^1 + \sinh\lambda z^1 \sin\lambda z}{\cosh \lambda W + \cos\lambda W} \text{ ; hinged ends} \quad (3)$$

$$\frac{2\lambda^2 M}{p} = \frac{1}{\sinh\lambda W + \sin\lambda W} (\sinh\lambda z\cos\lambda z^1 + \cos\lambda z\sinh\lambda z^1$$

$$-\sin\lambda z\cosh\lambda z^1 - \cosh\lambda z\sin\lambda z^1); \text{ fixed ends} \quad (4)$$

in which M = bending moment per unit width; p = uniformly distributed load per unit width applied on the beam; z = distance from the left ice edge; z^1 = distance from the right ice edge = W - z; and λ is defined by

$$\lambda = \sqrt[4]{\gamma/4EI} \quad (5)$$

in which E = elastic modulus of ice; and I = moment of inertia of ice cover per unit width = $h_i^3/12$.

Eqs. 3 and 4 may be used to study the location of maximum M and the uplift pressure necessary to cause cracking of the cover. First, the case $\lambda W \to \infty$ is considered. Eqs 3 and 4 reduce to

$$\frac{2\lambda^2 M}{p} = e^{-\lambda z}\sin\lambda z, \quad \text{hinged ends} \quad (6)$$

$$\frac{2\lambda^2 M}{p} = e^{-\lambda z}(\sin\lambda z - \cos\lambda z), \quad \text{fixed ends} \qquad (7)$$

These expressions are identical to Billfalk's (1981) for the infinitely wide channel case.

For finite channel widths, Eqs. 3 and 4, along with corresponding equations for ice deflection (Hetenyi, 1946) can be used to determine moment and deflection variations across the channel. Typical results for hinged ends are shown in Figs. 2 and 3. Fig. 2 shows that maximum bending occurs at mid-stream for $\lambda W \leq 3.0$ which suggests that only one central crack should form in this case. However, as λW increases above 3, the maximum bending moments are no longer located at mid-stream which implies that two longitudinal cracks should form, each located a distance l_s off the respective channel end. For the case of fixed ends the calculations have indicated that $l_s = 0$, i.e., maximum bending occurs at the channel edges.

Figure 4 shows the variation of l_s/W with λW while Fig. 5 gives the uplift pressure required to cause crack formation, p_f, as a function of λW as well as ice thickness and ice properties (note that σ_i = flexural strength of the ice cover). Figs. 4 and 5 indicate that an ice cover may be considered "infinitely" wide if $\lambda W \geq 6$.

The present results also apply to the case of an ice cover subjected to a drop in the water level, provided the bottom of the cover is everywhere in contact with water. This property was utilized by Billfalk (1981) to test his analysis and obtain good agreement with observation, using E = 6.5 GPa. The latter figure is practically the same as 6.8 GPa, recommended by Gold (1971) for good-quality freshwater ice.

Where cracking is the result of uplift pressures, as happens near the time of breakup, it is not possible to know before hand whether the end supports are fixed or hinged. However, when longitudinal cracks are offset, i.e., they are located some distance off the edges ("hinge" cracks), one could assume hinged supports.

Where no cracks are present, even though the ice cover is detached from the river banks, one must assume that either the end supports were fixed, or the adhesion of the ice to the banks was too low to permit development of hinge cracks. In the writer's experience, longitudinal cracks are usually offset so that the hinged support type would seem to be a common occurrence.

Another complication that may arise in nature may be due to creep effects. Ice is known to be a viscoelastic material that only exhibits elastic behaviour during brief loading times. However, the creep characteristics of ice are not well understood at present while the loading history of the ice cover under the present conditions is difficult to determine. As shown in Appendix A, the loading time is of the order of a few hours which guarantees substantial creep effects. A simple empirical approach in this case is to use the results of the elastic analysis but introduce reduced values of E and σ_i.

From observations of crack locations in the Thames River (Ontario), a value of E = 1.4 GPa has been deduced. This is about five times less than the elastic modulus of good-quality ice subjected to rapid loading. The difference is large but can be attributed to creep effects. In Appendix A it is shown that the ice cover is subjected to an increasing distributed load while the time to failure is of the order of a few hours. Sinha's results (1977) with small ice specimens subjected to constant compressive stresses, indicate similar reductions in the apparent value of E for similar loading times. Though the respective loading configurations and histories differ, the approximate coincidence of Sinha's results with the present ones supports the hypothesis that creep is largely responsible for the low value of E proposed herein.

2.3 Case Studies and Examples

Using E = 1.4 GPa, we now proceed to describe a few field observations and compare them to prediction.

(1) Thames River at Thamesville, 1981 and 1982. Observed $l_s \approx 5.0$ m; $h_i = 0.32$ m; $W = 40$ m. From Eq. 5 we find $\lambda = 0.16$ m^{-1} and $\lambda W = 6.4$ which exceeds 6.0 so that the infinite-width formulae apply. It follows that the predicted value of l_s is equal to $\pi/4\lambda$ (see Eq. 6), i.e., $l_s = 4.9$ m which is close to the observed value.

(2) Thames River near Louisville, 1983. Observed $l_s \approx 2.0$ m; $h_i = 0.11$ m; $W \approx 55$ m. We find $\lambda = 0.35$ m^{-1} and $\lambda W = 19.5$. Therefore, predicted $l_s = \pi/4\lambda = 2.2$ m which is close to the observed value.

(3) For several Manitoba streams, it has been observed that a single central crack occurs for widths less than 30 m (J. Wedel, personal communication). Fig. 4 then implies that λW should be less than 3.0. Therefore λ should not exceed $3/30 = 0.1$ m^{-1}. Using Eq. 5 gives $h_i > 0.6$ m which was indeed the case for the streams under consideration (J. Weddel, personal communcation).

(4) Grand River near Leggatt, 1982. A single, mid-channel crack was observed in this reach prior to breakup. Accurate values of h_i and W are not available. Ice thickness has been estimated as 0.45 m from measurements elsewhere on the Grand River. The channel width has been assumed to be 27 m, a value measured under open water conditions at a stage similar to that which prevailed when the crack was observed. Putting $E = 1.4$ GPa and $h_i = 0.45$ m in Eq. 5 gives $\lambda = 0.12$ m^{-1} and $\lambda W = 3.3$ which, from Fig. 4, suggests that two cracks should form, contrary to what was observed. However, the accuracy of h_i and W is such that λW could easily have been 3 or less which would indicate only one crack formed. Moreover, inspection of Fig. 2 indicates that when λW is between 3 and 3.5, the maximum bending moment is only slightly more than the central moment. If, as is often the case,

h_i varies somewhat across the stream, being thinner near the centre, a central crack would form even if $\lambda W > 3$ (note that bending stress varies as h_i^{-2}).

As an example of applying the present results, let h_i = 0.50 m, W = 50 m, E = 1.4 GPa and σ_i = 600 KPa; then Eq. 5 gives

$$\lambda = \{9.81 \times 10^3/(4 \times 1.4 \times 10^9 \times 0.5^3/12)\}^{1/4} = 0.11 \text{ m}^{-1}.$$

Hence $\lambda W = 5.7$ and $\lambda h_i = 0.057$. From Fig. 5, we find that $p_f/\sigma_i(\lambda h_i)^2 = 1.04$, hence p_f = 2.0 kPa. After formation of cracks, the ice cover would float at an elevation that would exceed the pre-stressing one by $2.0 \times 10^3/9.8 \times 10^3$ = 0.21 m. Fig. 3 indicates that the maximum deflection is about $1.1\ p_f/\lambda = 1.1 \times 0.21$ = 0.23 m which is less than $s_i h_i$ (=.92 x .5 = 0.46 m), as is required for the theory to apply. For $\lambda W = 5.7$, Fig. 4 gives l_s/W = 0.137, hence $l_s = 50 \times 0.137 = 6.9$ m.

3.0 TRANSVERSE CRACKS - BENDING ON VERTICAL PLANES

Transverse cracks are often observed in the river ice cover when breakup is imminent. The mechanisms responsible for transverse cracking are not clearly understood at present and can only be studied by consideration of the spacing of the cracks and the stresses required to cause cracking. An obvious candidate is bending of the ice on vertical planes by an advancing flood wave. This possibility is explored in this section.

3.1 Physical Considerations and Assumptions

When runoff is increased, the ice cover will first crack longitudinally and eventually detach from the river banks. Once this

has occurred, the ice cover will become subject to bending on vertical planes, owing to the shape of the water surface. The latter may exhibit a wave-like form that travels in the downstream direction. The wave could be the result of increasing runoff or ice jam release or a combination of these effects. With reference to Fig. 6, the total upward pressure applied on the ice cover can be shown to be equal to $\gamma\delta - \gamma w$ for the region where the water level is below the top of the ice cover ($x \geq 0$); and equal to $\gamma (1 - s_i)h_i$ where the top ice surface is submerged ($x < 0$). Therefore, for $x \geq 0$, the ice cover may be considered a beam subjected to a distributed load ($= \gamma\delta$) and supported by an elastic foundation of modulus equal to γ. For $x < 0$, the ice cover acts as a free beam subjected to the uniform load $\gamma(1 - s_i)h_i$. Because δ and l_o (= length of ice cover submergence, see Fig. 6) are time-dependent, w is also time-dependent, i.e., $w = w(x,t)$. It follows that the differential equation describing w (e.g., see Flügge 1962) should include a term proportional to the vertical ice acceleration, $\frac{\partial^2 w}{\partial t^2}$. Based on an order of magnitude analysis, Billfalk (1982b) argued that this term can be neglected, so that any instantaneous distribution of w is produced by the static loading $\gamma\delta(x)$ that prevails at the same time. This assumption is retained herein (see Appendix B).

To obtain $\delta(x)$, the form of the water surface should, strictly speaking, be determined from fluid dynamic considerations. However, this is a highly complex task and a first approximation is to use an assumed shape of the water surface profile. This problem was first considered by Billfalk (1982a) who used a linear water surface. However, Billfalk's analysis did not consider the loss of the elastic "foundation" along the submerged portion of the ice cover or the effect of the ice deflection on the location of point A (Fig. 6).

Herein, these effects are taken into account and a more realistic water surface shape is assumed, i.e.,

$$\delta(x) = \delta_0 e^{-\mu\lambda x} \tag{8}$$

in which δ_0 = value of δ at $x = 0$; and μ is a dimensionless coefficient.

3.2 Analytical Relationships

Details of the solution are given in Appendix C while the main relationships are reproduced below.

for $x \geq 0$: $$\frac{\lambda^2 M}{q_s} = e^{-\xi}(\alpha_1 \sin\xi + \alpha_2 \cos\xi) - \alpha_3 e^{-\mu\xi} \tag{9}$$

in which $\xi = \lambda x$; $q_s = \gamma(1 - s_i)h_i$; and $\alpha_1, \alpha_2, \alpha_3$ are dimensionless coefficients defined by

$$\alpha_1 = \frac{(1-\mu)(1+\psi)^2}{(\mu-1)^2 + 1} - \psi\left(1 + \frac{\psi}{2}\right) \tag{10}$$

$$\alpha_2 = \frac{(1+\psi)^2}{(\mu-1)^2 + 1} - \frac{\psi^2}{2} \tag{11}$$

$$\alpha_3 = \frac{(1+\psi)^2}{(\mu-1)^2 + 1} \tag{12}$$

$$\psi = \lambda l_0 \tag{13}$$

Of interest are also the deflections w_e (at $x = -l_0$, i.e., at the ice edge) and w_0 (at $x = 0$):

$$\frac{\gamma w_0}{q_s} = \frac{\gamma \delta_0}{q_s} - 1 \tag{14}$$

$$\frac{\gamma\delta_o}{q_s} = \frac{(\mu+1)^2 + 1}{\mu^2} (1 + \psi)^2 \qquad (15)$$

$$\frac{\gamma w_e}{q_s} = \frac{\gamma w_o}{q_s} + 2\psi (1+\psi)\left(\frac{1+\psi}{\mu} + \psi\right) + \frac{\psi^4}{2} \qquad (16)$$

Eq. 14 expresses the condition that the water surface and the top ice surface intersect at x = 0. If l_o (and ψ) are set equal to zero in the above equations, we will obtain the solution for the case where the edge of the ice cover is at the threshold of submergence.

However, if $l_o = 0$ and the ice cover is still emerging above the water level (i.e., $\gamma w_o/q_s < (\gamma\delta_o/q_s) - 1$), the solution becomes

$$\frac{\lambda^2 M}{\gamma\delta_o} = \frac{\mu^2}{4+\mu^4} \left[e^{-\xi} \{(1-\mu) \sin\xi + \cos\xi\} - e^{-\mu\xi}\right] \qquad (17)$$

$$\frac{w_o}{\delta_o} = \frac{2(\mu+1)}{(\mu+1)^2 + 1} \qquad (18)$$

It is noted that the analysis ignores the deformation of the water surface that takes place near the ice edge due to local stagnation effects. This, however, is a rather localized occurrence and should not greatly influence the results.

Figure 7 shows dimensionless plots of maximum bending moment, edge deflection and crack location versus μ, prior to

submergence of the ice cover. Plots of bending moment versus x have indicated that the moment drops to negligible values beyond distances of $6/\lambda$ to $10/\lambda$. When a part of the ice cover is submerged, Eqs. 9-16 apply. Figures 8 and 9 show dimensionless moments and crack locations plotted versus μ with ψ as a parameter while more detailed results are presented in Table 1.

3.3 Examples

As an example, consider a 0.5 m thick ice cover with σ_i = 600 KPa and E = 6.8 GPa (because the wave travels relatively fast, there is little time for creep and thence for reduction of the apparent modulus of elasticity. Then, from Eq. 5, $\lambda = 0.077\ m^{-1}$ and $\lambda h_i = 0.038$. The bending moment, M_f (per unit width) required to cause a crack is

$$M_f = \frac{1}{6}\ \sigma_i h_i^2 \tag{19}$$

and the dimensionless quantity $\lambda^2 M_f/q_s$ works out to

$$m_f = \lambda^2 M_f/q_s = \frac{1}{6}\ (\lambda h_i)^2\ \frac{\sigma_i}{\gamma(1-s_i)h_i} \tag{20}$$

For the present example, m_f = 0.37. Inspection of Fig. 8 suggests that, to effect cracking without submerging the ice cover (ψ = 0), the flood wave must have a value of μ that is no more than 0.25. For μ = 0.25, Eqs. 14-16 (or Table 1) indicate that $w_e = w_o$ = 1.60 m and δ_o = 1.64 m which are large but not implausible values. The crack location ($x = l_c$) can be determined from Fig. 9, i.e., λl_c = 2.2 and l_c = 28.6 m so that l_c/h_i = 57. The "average" slope $\overline{\Delta S}$, of the

wave can be defined over a distance x_o such that the value of δ at x_o becomes (say) 2% of δ_o *. Then

$$\overline{\Delta S} = 0.25 \mu \lambda \delta_o \qquad (21)$$

and works out to $\overline{\Delta S} = 0.008$. This value is rather large and it is questionable whether it can normally occur in nature, unless the wave is a surge caused by ice jam release. As the wave moves downstream, the value of μ must decrease due to subsidence. If μ were, for example, equal to 0.10, Fig. 8 suggests that a crack would form before the edge of the ice cover reaches the water surface. Then, the graphs of Fig. 7 would apply. For $\mu = 0.1$, $\max|M|\lambda^2/\gamma\delta_o = 0.002$ and $\max|M|\lambda^2/q_s = 0.002\ \gamma\delta_o/q_s$. To effect cracking, the latter quantity should be equal to m_f, i.e., 0.37. Hence $\gamma\delta_o/q_s = 185$ and thence $\delta_o = 7.4$ m which is an extreme value, unlikely to be encountered in nature. The corresponding value of l_c is also given in Fig. 7 as $\lambda l_c = 2.55$. Hence $l_c = 33.1$ m or $l_c/h_i = 66$ and $\Delta S = 0.014$ which, too, is implausibly large.

Another example can be worked out if μ is set equal to 1.00. Fig. 8 indicates that, for $\psi = 0$, the value of m is 0.21 which is less than 0.37 and thus the ice cover will not fracture without submergence. Using Table 1, the required value of ψ can be determined by interpolation. This gives $\psi = 0.22$ and $\lambda l_o = 1.63$. Therefore, $l_c = 21.1$ m and $l_c/h_i = 42$. Moreover, Eqs. 14-16 indicate that $\delta_o = 0.30$ m, $w_o = 0.26$ m and $w_e = 0.29$ m, all of which are plausible. The average slope (Eq. 21) is 0.006 which again would be expected to occur under jam release conditions.

---

* Note that this slope is in addition to the channel slope under steady flow conditions.

3.4 Implications

The preceding analysis has shown that advancing flood waves can break an ice cover by bending on vertical planes provided the wave slope (i.e., the slope in excess of the steady-state value) is about 5×10^{-3} or more*. Such slopes are rather extreme and unlikely to be produced by runoff alone; they could, however, prevail for a brief time after the release of a large ice jam. At the same time, it should be recognized that major jam releases are often attended by very large flow velocities and shear stresses. It is possible, therefore, that an ice cover will be destroyed by hydrodynamic forces or by the advancing ice jam well before it can be fractured by vertical bending. The mechanisms involved in this type of breaking are unclear at present and thus no quantitative analysis is possible.

4.0 TRANSVERSE CRACKS - BENDING ON "HORIZONTAL" PLANES

Shulyakovskii (1972) proposed a breakup mechanism which would result in transverse cracks due to stressing on planes parallel to the water surface (herein called, with some license, "horizontal" planes for simplicity). This mechanism is illustrated in Fig. 10 where it is shown that stresses develop in the ice due to the accumulated effects of the flow shear stress and the downslope component of the weight of the ice cover. In a straight river, only compressive stresses can develop but, in a meandering channel, shear stresses and bending moments are also present. It can be shown that tensile stresses caused by bending are the most likely to cause fracture of the ice cover. Moreover, an order-of-magnitude calculation has indicated that cracks caused by horizontal bending would be spaced

---

* The required slope is roughly proportional to $\sqrt{\sigma_i}$. If σ_i drops to as low a value as 100 kPa due to thermal deterioration, the limiting wave slope would be 2×10^{-3} which too is a large value.

very far apart relative to what was determined for the case of vertical bending. Transverse crack patterns with average spacings of 1,000 to 1,600 ice thicknesses have been observed recently in the lower Thames River (Ontario). An example is shown in Fig. 11 while the statistical distributions of l_i (= distance between consecutive cracks) are illustrated in Fig. 12.

To test whether horizontal bending might have been responsible for the Thames River results, it is necessary to estimate the associated bending moments. This is not a simple matter because the forces transferred between adjacent ice sheets depend on local channel geometry and re-alignment of sheets after crack formation. With reference to Fig. 13, a crude estimate can be obtained by assuming that crack C forms solely as a result of (a) bending caused by tangential forces along the arc BC; and (b) bending caused by the force transmitted from sheet AB to sheet BC. Contributions from ice sheets farther upstream, are neglected. The bending moment at C is then (see Appendix D for derivation)

$$M = 2 \tau W_i a \qquad (22)$$

in which W_i = width of ice cover; a = shaded area in Fig. 13; and $\tau = \tau_i + \gamma s_i h_i S$, with τ_i = flow shear stress applied on the underside of the ice cover; S = slope of water surface. When a crack forms, M is equal to $\sigma_i h_i W_i^2/6$. Using Eq. 22, the flexural strength, σ_i can be estimated from

$$\sigma_i = 12 \left(\frac{a}{h_i W_i}\right) \tau \qquad (23)$$

Table 2 summarizes observed characteristics of the Thames River ice sheets and estimated values of σ_i based on Eq. 23. The latter range from 60 to 100 kPa which is low relative to 600 kPa, a common flexural strength value for good-quality ice, determined by the well-known beam test (Frankenstein 1961; Korzhavin 1971; Butyagin 1972). However, the value of σ_i has been found to decrease with specimen size. For the present loading configuration, Butyagin's (1972) results suggest a reduction factor of at least 3 and possibly as much as 5 for the flexural strength of the entire ice cover, relative to that obtained from beam tests. This would bring σ_i up to at least 180-300 kPa which is well above the lower limit of σ_i measured near the time of breakup ($\simeq$ 100 kPa - Frankenstein 1961). Reductions in strength could also result from creep effects or from penetrating short wave radiation (e.g., see Bulatov 1972; Ashton 1983).

In conclusion, it may be stated that "horizontal" bending could account for the crack patterns observed in the Thames River. It may also be noted that this mechanism does not require "surge" action as it can be effective with relatively low values of τ (Table 2).

5.0 DISCUSSION

The preceding analysis has illustrated some of the patterns by which an ice cover is likely to be fractured before it is set in motion. It is emphasized that patterns not considered herein are also possible, for example, intense thermal deterioriation can cause large open leads and frequent discontinuities in the ice cover. Thus, the present results are most applicable to the premature breakup, i.e., where conditions of rapid runoff prevail with little heat input to the ice cover.

The first occurrence of fracture appears soon after the discharge begins to increase and is manifested by the formation of longitudinal cracks that , in streams of fair widths, are parallel and close to the banks. However, as the channel width decreases, the two

cracks may shift towards the centre and eventually merge into a single, mid-channel crack. The relative location of the longitudinal or "hinge" cracks, l_s/W, is governed by the parameter λW, i.e., it depends on channel width as well as ice thickness, density and modulus of elasticity. In the case of a single crack, continuing rise in the water level is likely to lift the free ice edges at midstream and submerge the two ice strips if the far edges remain attached to the river banks (e.g., see Fig. 14). Eventually, heat transfer will cause detachment and free flotation of the side strips.

In the more usual case where two hinge cracks form, the middle portion of the ice cover will rise with the water level and eventually lose any support that might have been provided at points of contact with the side strips. At this time, the ice cover is still unable to move but is subject to relatively large stresses owing to loss of boundary support. In turn, these stresses may lead to formation of transverse cracks.

Two mechanisms of transverse crack formation have been studied herein. The first mechanism involves bending on vertical planes due to an advancing water wave that tends to lift and deform the ice cover. Analysis suggests that rather steep waves are necessary to cause fracture. Except for very steep and small streams, such waves can only occur artificially* or following the release of a major ice jam upstream.

A different mechanism of transverse crack formation produces ice sheets of the order of thousands of ice thicknesses long. This is likely related to "horizontal" bending which arises essentially from the meandering planform of natural streams. This type of fracture does not require wave action, though it would be assisted by it through augmented flow shear stresses.

The present study has considered some of the phenomena associated with early breakup phases, with focus on mechanisms that

---

* e.g., by sudden reservoir releases

can reduce the ice cover to a sequence of separate ice sheets. Further breakage and the onset of jamming may then result from increased stage and channel width which allows some of the ice sheets to move (e.g., see Beltaos 1984).

A more violent type of ice cover destruction may result from releases of major ice jams (Gerard et al. 1984; Beltaos 1985 - Unpublished data). In this case, a "breaking front" develops with a sharp transition between broken and intact ice. Front speeds of up to 5 m/s have been reported. It is not known what mechanisms are at work and thus it is difficult to consider the conditions under which the front would keep moving or eventually be arrested, leading to a new jam. It should be recognized, however, that flow velocities during ice jam surges can be 10 or more times the ordinary steady-state values which would result in amplification of the hydrodynamic forces by a factor of 100 or more. Therefore, processes that ordinarily have little effect on the ice cover, may contribute to its breaking during surge action.

6.0 SUMMARY

Two frequently observed types of early fracture of the river ice cover have been studied, namely the longitudinal and transverse cracks. Longitudinal cracks result from uplift pressure caused by increasing discharge. These cracks appear soon after the start of runoff and usually occur in pairs, one near each bank. A single central crack occurs when ice thickness is large or channel width is small.

Where two longitudinal cracks form, the central portion of the cover detaches eventually from the side strips, as the flow increases. Transverse cracks may then form, by bending on vertical or horizontal planes. Vertical bending requires rather extreme water surface slopes, unlikely to occur in most streams, except during surges from ice jam releases. However, during surge action,

hydrodynamic forces are greatly amplified so that vertical bending, if it occurs, could be of minor significance in ice breaking.

Horizontal bending results principally from flow shear and the meandering planform of natural streams. Transverse crack patterns, observed in the Thames River favour horizontal bending as the formative process.

ACKNOWLEDGEMENTS

Most of the numerical calculations needed for the present results were performed by J. Wong of the Hydraulics Division. Review comments by Dr. T.M. Dick, Chief, Hydraulics Divison and Dr. Y.L. Lau, Head, Environmental Hydraulics Section, are appreciated.

REFERENCES

Ashton, G.D., 1983. First Generation Model of Ice Deterioration. Proceedings of Conference on Frontiers in Hydraulic Engineering, ASCE, Cambridge, Mass. pp. 273-278.

Beltaos, S., 1984. A Conceptual Model of River Ice Breakup. Canadian Journal of Civil Engineering, Vol. 1, No. 3, pp. 516-529.

Billfalk, L., 1981. Formation of Shore Cracks in Ice Covers Due to Changes in the Water Level. Proceedings, IAHR International Symposium on Ice, Quebec, Canada, Vol. II, pp. 650-660.

Billfalk, L., 1982a. Breakup of Solid Ice Covers Due to Rapid Water Level Variations. U.S. Army CRREL Report 82-3, Hanover, NH.

Billfalk, L. 1982b. Breakup of Solid Ice Covers due to Rapid Water Level Variations - A Note on Dynamic Effects. Swedish State Powr Board, Technical Note, Alvkarleby, Sweden, 6 p.

Bulatov, S.N., 1972, Computation of the Strength of the Melting Ice Cover of Rivers and Reservoirs and Forecasting of the Time of Its Erosion. Proc., IAHS Symposium on the Role of Snow and Ice in Hydrology, Vol. I, Banff, IAHS-AISH Publication No. 107, pp. 575-581.

Butyagin, I.P., 1972, Strength of Ice and Ice Cover (Nature Research on the Rivers of Siberia), U.S. Army CRREL, Draft Translation 327, Hanover, N.H.

Flügge, W. (editor-in-chief), 1962. Handbook of Engineering Mechanics. McGraw-Hill Book Co., New York, Toronto, London.

Frankenstein, G.E., 1961, Strength Data on Lake Ice, U.S. Army SIPRE Technical Report 80, Hanover, N.H.

Gerard, R., T.D. Kent, R. Janowicz, and R.O. Lyons. 1984. Ice Regime Reconnaissance, Yukon River, Yukon. Cold Regions Eng. Spec. Conf., Edmonton, Vol. III, pp. 1059-1073.

Gold, L.W., 1971. Use of Ice Covers for Transportation. Canadian Geotechnical Journal, 8, pp. 170-181.

Hetenyi, M., 1946. Beams on Elastic Foundation. Ann Arbor: The University of Michigan Press.

Korzhavin, K.N., 1971. Action of Ice on Engineering Structures, U.S. Army CRREL AD 723 169, Hanover, N.H.

Shulyakovskii, L.G., 1972. On a model of the breakup process. Soviet Hydrology: Selected Papers, Issue No. 1, pp. 21-27.

Sinha, N.K. 1977. Effective Elasticity of Ice. Proceedings of Workshop on the Mechanical Properties of Ice, NRCC Technical Memorandum No. 121, pp. 112-123.

Sorensen, C. 1978. Interaction between Floating Ice Sheets and Sloping Structures. Institute of Hydrodynamics and Hydraulic Engineering, Techn. Univ. of Denmark, Series Paper No. 19.

TABLE 1
Results of "Vertical Bending" Analysis -

Full Submergence of Ice Cover

ψ	μ	$\frac{\lambda^2 \max\|M\|}{q_s}$	λl_c	$\frac{w_o}{(1-s_i)h_i}$	$\frac{w_e}{(1-s_i)h_i}$	$\frac{\overline{\Delta S}}{(1-s_i)\lambda h_i}$
0	0.25	0.368	2.20	40.00	40.00	2.56
	0.50	0.291	1.90	12.00	12.00	1.63
	1.00	0.208	1 57	4.00	4.00	1.25
	1.50	0.162	1.40	2.22	2.22	1.21
	2.00	0.132	1.30	1.50	1.50	1.25
	3.00	0.096	1.15	0.89	0.89	1.42
	4.00	0.075	1.05	0.63	0.63	1.63
	6.00	0.052	1.00	0.39	0.39	2.09
	10.00	0.032	0.90	0.22	0.22	3.05
0.50	0.25	0.895	2.35	91.25	101.00	5.77
	0.50	0.764	2.05	28.25	33.53	3.66
	1.00	0.623	1.75	10.25	13.28	2.81
	1.50	0.545	1.60	6.25	8.53	2.72
	2.00	0.495	1.50	4.63	6.53	2.82
	3.00	0.434	1.40	3.25	4.78	3.19
	4.00	0.397	1.30	2.66	4.00	3.67
	6.00	0.355	1.25	2.13	3.28	4.70
	10.00	0.316	1.15	1.75	2.75	6.88
1.00	0.25	1.646	2.70	163.00	199.50	10.25
	0.50	1.452	2.40	51.00	71.50	6.50
	1.00	1.248	2.10	19.00	31.50	5.00
	1.50	1.137	1.95	11.89	21.72	4.84
	2.00	1.066	1.90	9.00	17.50	5.00
	3.00	0.979	1.75	6.56	13.72	5.67
	4.00	0.926	1.70	5.50	12.00	6.50
	6.00	0.864	1.60	4.56	10.39	8.34
	10.00	0.807	1.55	3.88	9.18	12.20

TABLE 1
(continued)

ψ	μ	$\frac{\lambda^2 \max \lvert M \rvert}{q_s}$	λl_c	$\frac{w_o}{(1-s_i)h_i}$	$\frac{w_e}{(1-s_i)h_i}$	$\frac{\overline{\Delta S}}{(1-s_i)\lambda h_i}$
1.50	0.25	2.623	3.05	255.30	344.00	16.02
	0.50	2.361	2.80	80.25	131.50	10.16
	1.00	2.093	2.50	30.25	62.78	7.81
	1.50	1.950	2.35	19.14	45.42	7.55
	2.00	1.858	2.30	14.63	37.78	7.82
	3.00	1.745	2.20	10.81	30.84	8.86
	4.00	1.678	2.10	9.16	27.63	10.16
	6.00	1.598	2.05	7.68	24.59	13.02
	10.00	1.522	2.00	6.63	22.28	19.08
2.00	0.25	3.828	3.50	368.00	544.00	23.06
	0.50	3.496	3.20	116.00	220.00	14.63
	1.00	3.164	2.95	44.00	112.00	11.25
	1.50	2.990	2.80	28.00	84.00	10.88
	2.00	2.879	2.70	21.50	71.50	11.25
	3.00	2.743	2.60	16.00	60.00	12.75
	4.00	2.661	2.55	13.63	54.63	14.63
	6.00	2.564	2.50	11.50	49.50	18.75
	10.00	2.471	2.40	9.98	45.58	27.45

TABLE 2
Characteristics of Ice Sheets Observed in the Thames River

Date of Observation	Reach Description	h_i (cm)	Approx. W_i (m)	Average l_i (m)	Average a (m^2)	Approx. τ (Pa)	Estimated σ_i (kPa)
Mar. 17/82	Upstream of Chatham; 30-40 km above river mouth	28	53	315	23,000	4.9	91
Feb. 14/84	Upstream of Chatham; 31-42 km above river mouth	30	57	307	23,950	5.8	97
Mar. 16/84	Upstream of Kent Bridge 51-56 km above river mouth	10	43	159	6,690	3.4	63

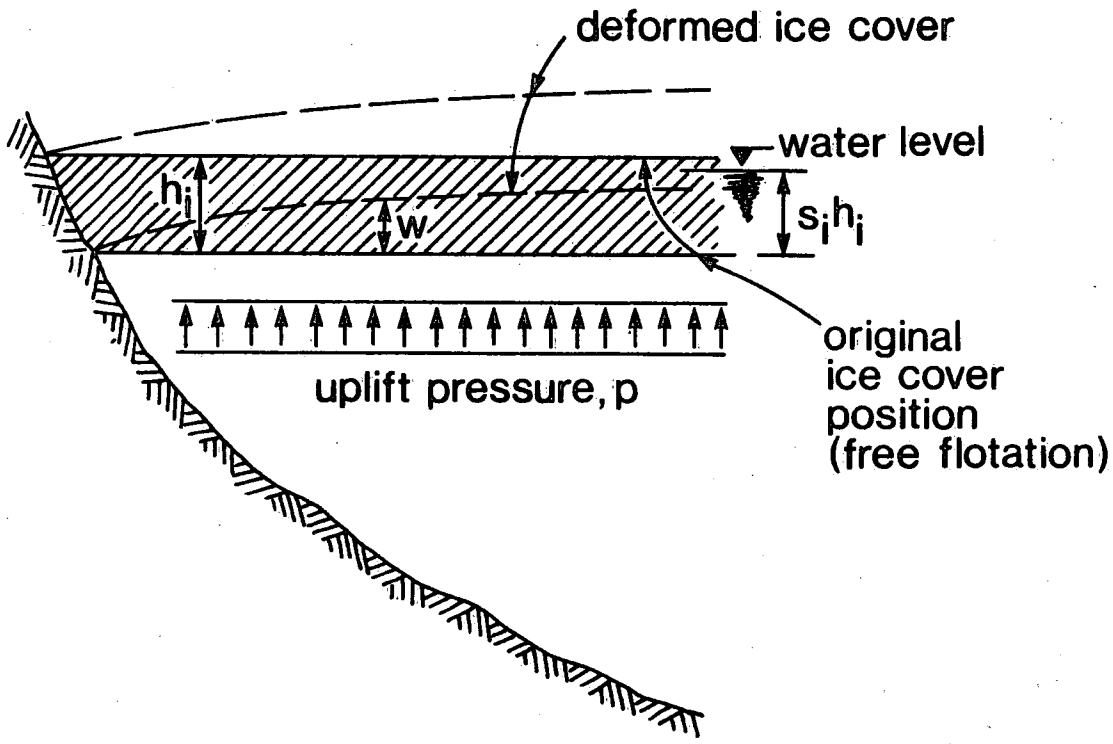

Fig. 1. Partial river section with ice cover, subjected to distributed load p.

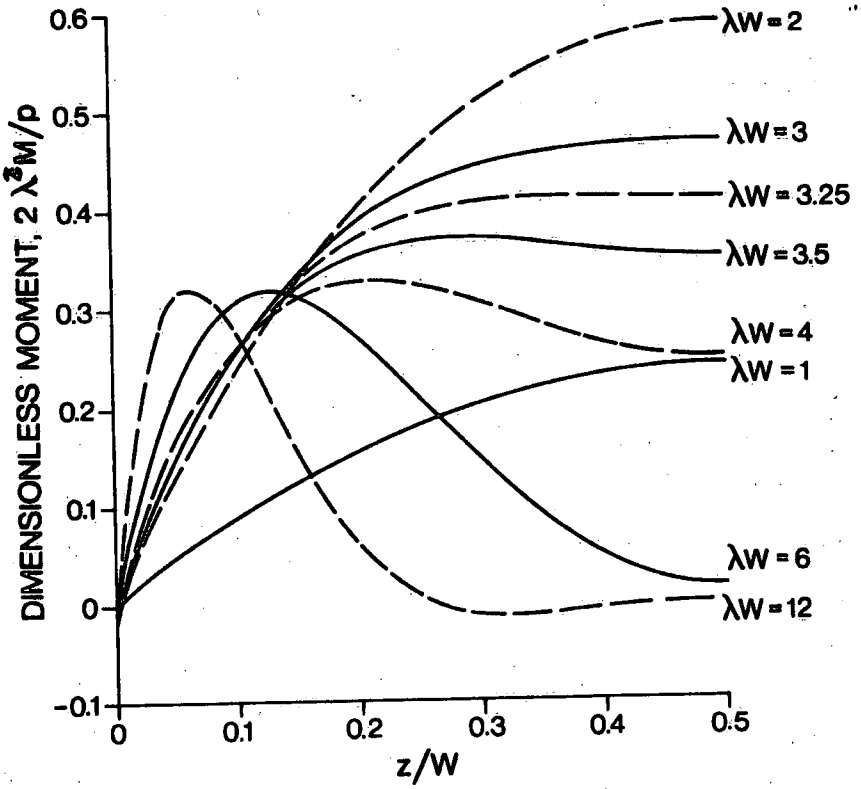

Fig. 2. Distribution of bending moment for hinged ends.

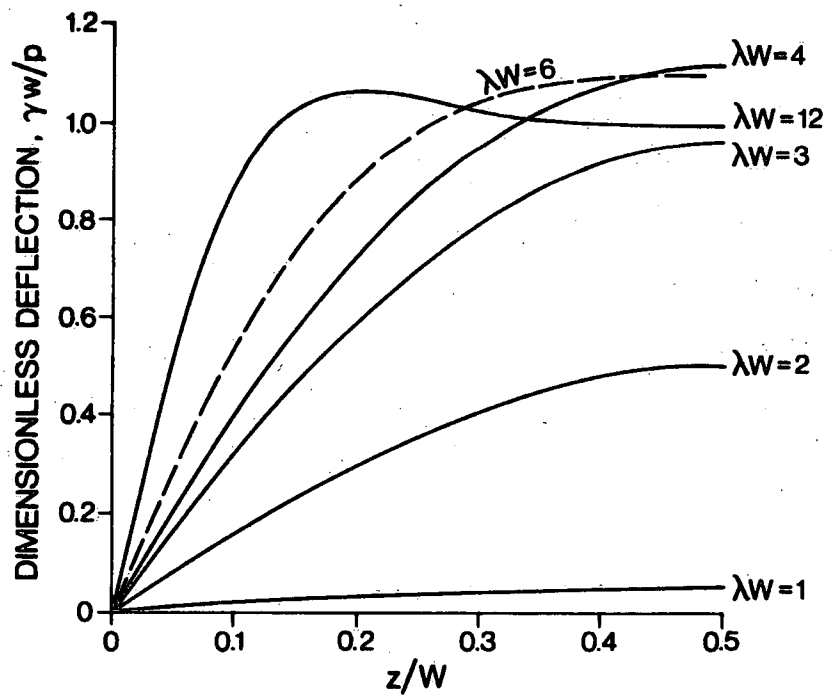

Fig. 3. Distribution of ice deflection for hinged ends.

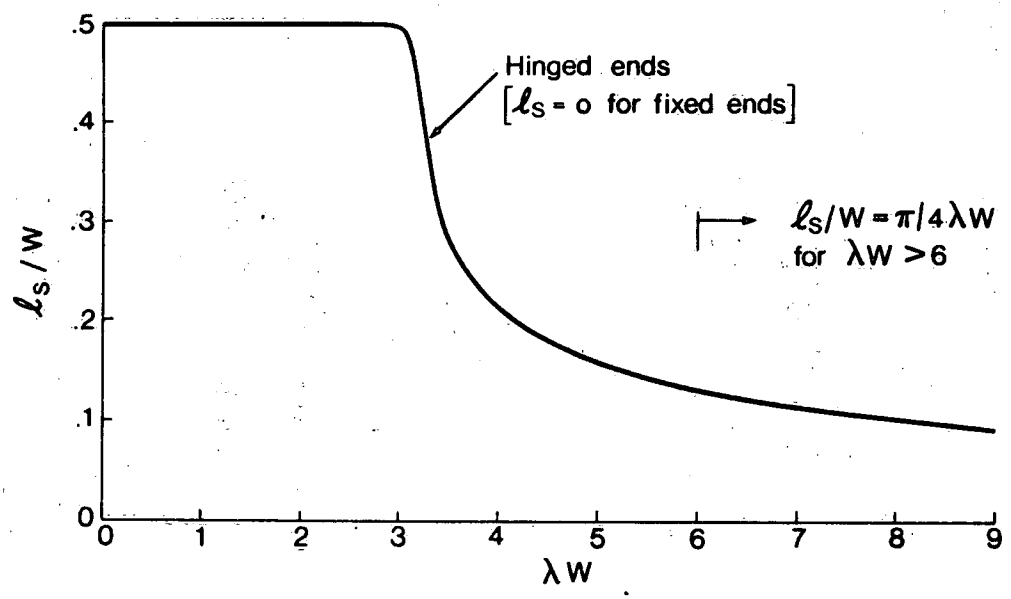

Fig. 4. Location of longitudinal cracks.

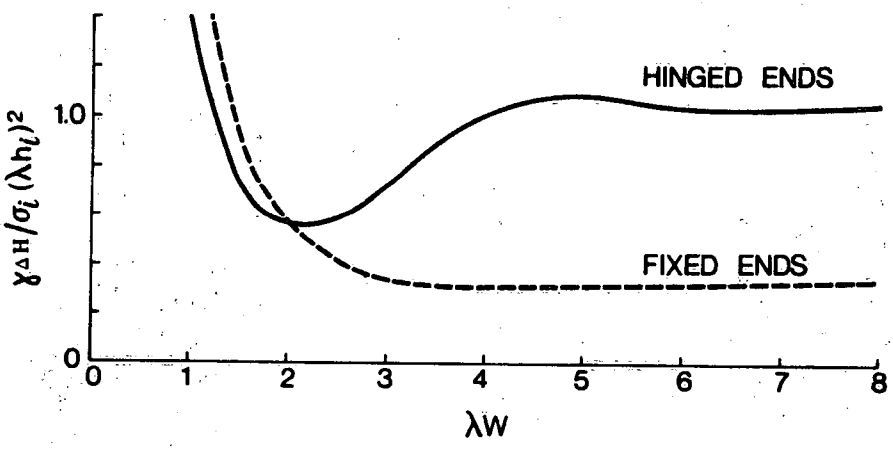

Fig. 5. Dimensionless uplift pressure required to cause longitudinal cracks.

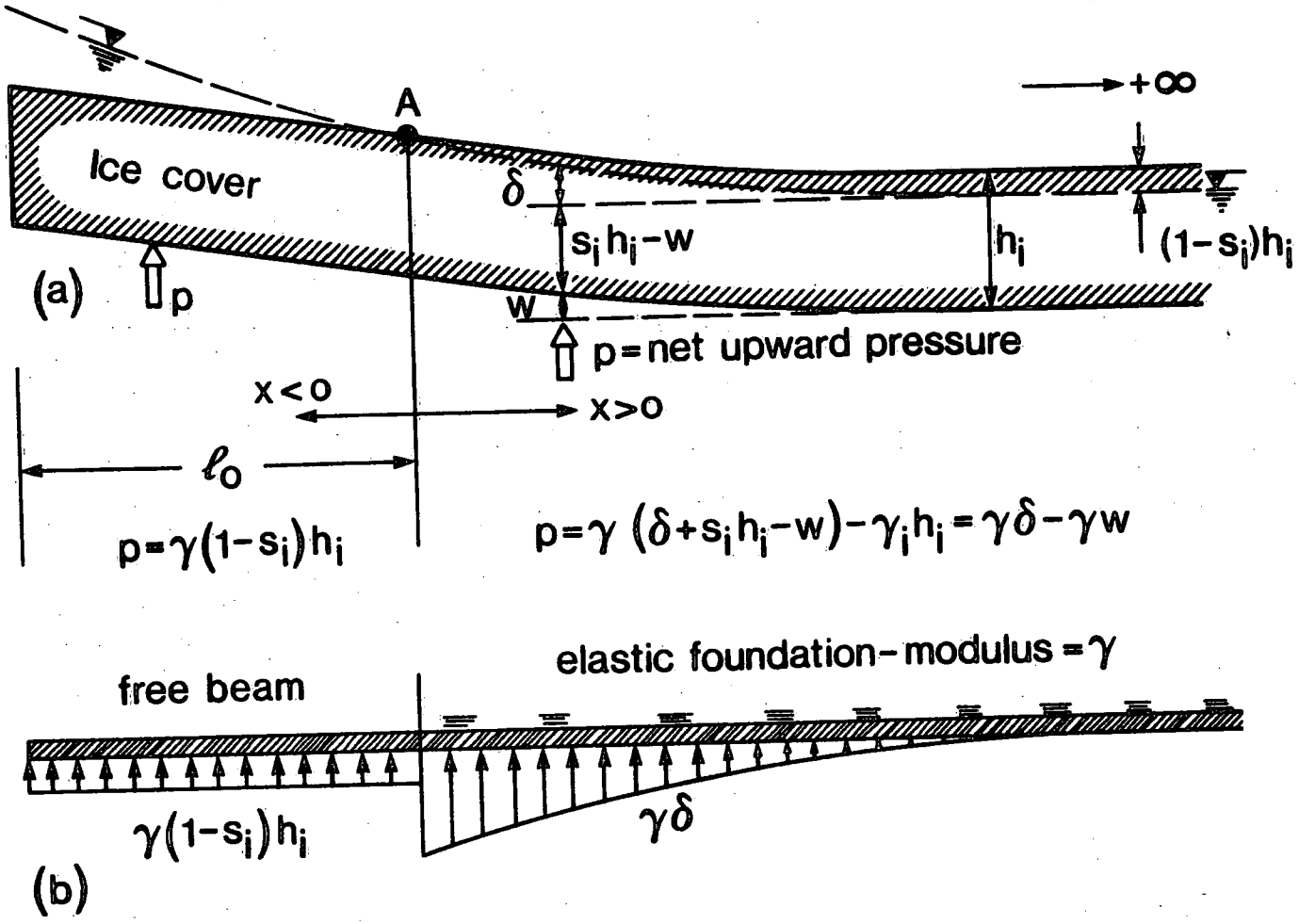

Fig. 6. Ice cover deformed by flood wave. a) Definition sketch;
b) Loading and support configurations

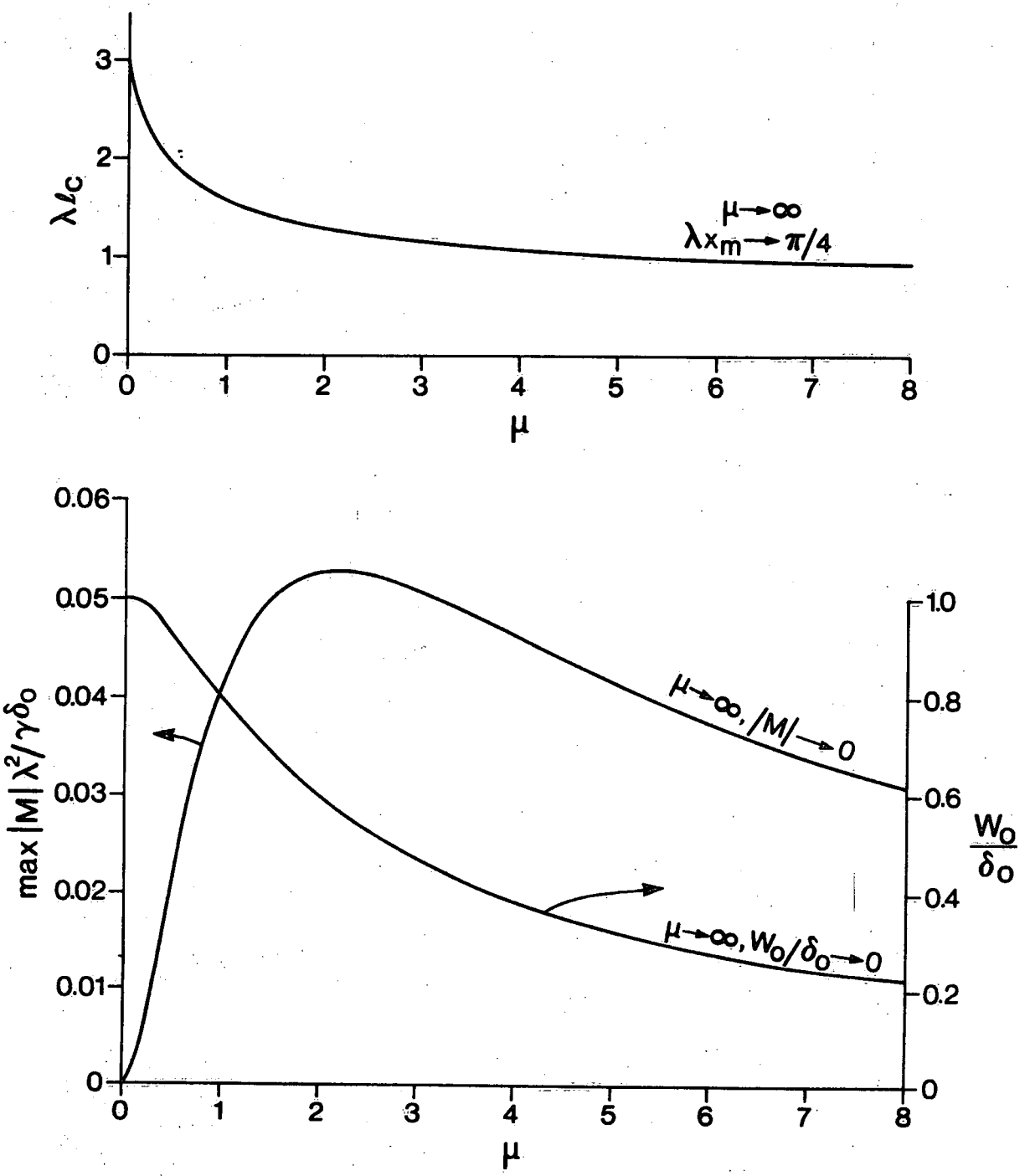

Fig. 7. Location and magnitude of maximum bending moments for non-submerged ice sheet; and relative edge deflection versus μ. Vertical bending case.

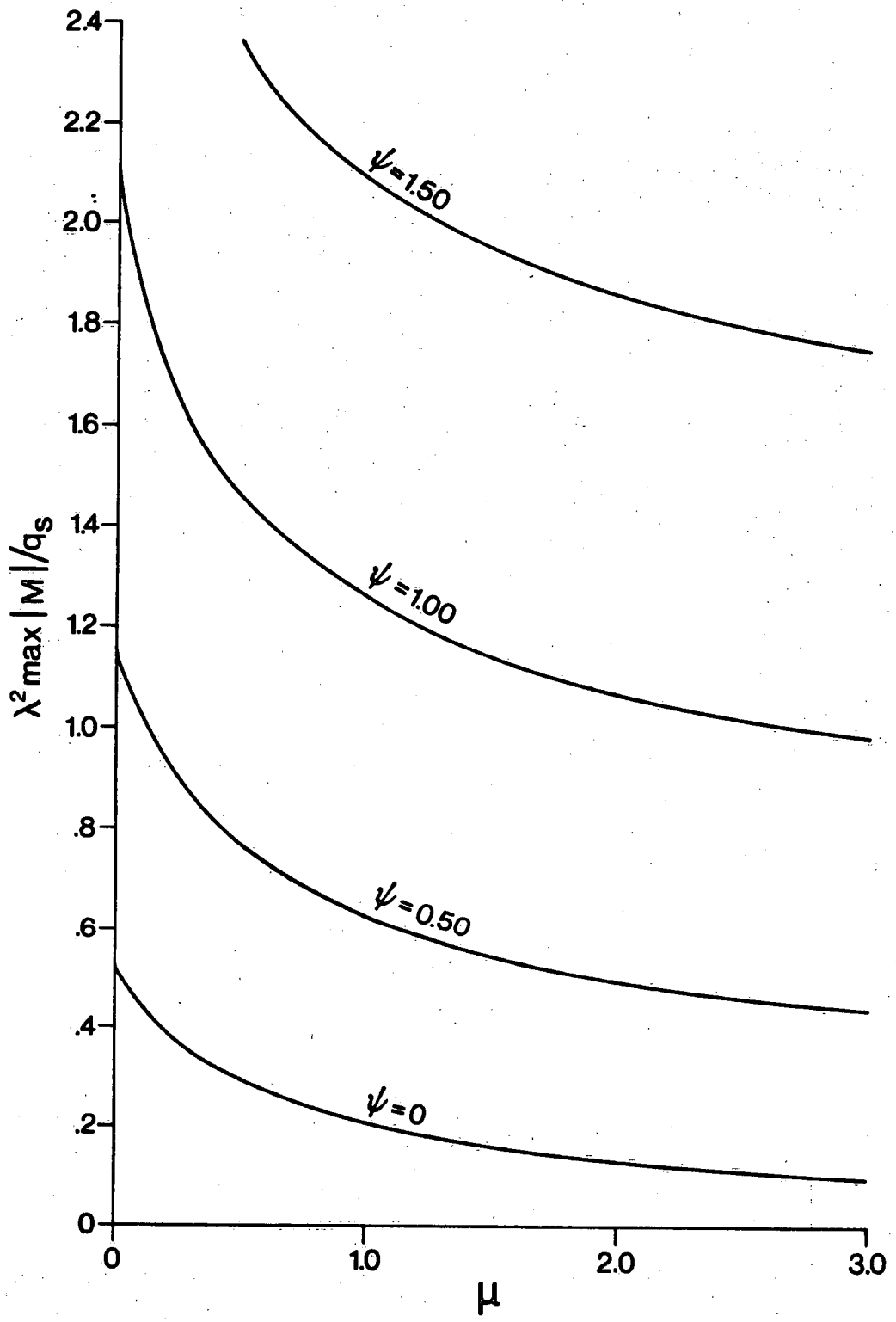

Fig. 8. Maximum bending moment for partly submerged ice sheet. Vertical bending case.

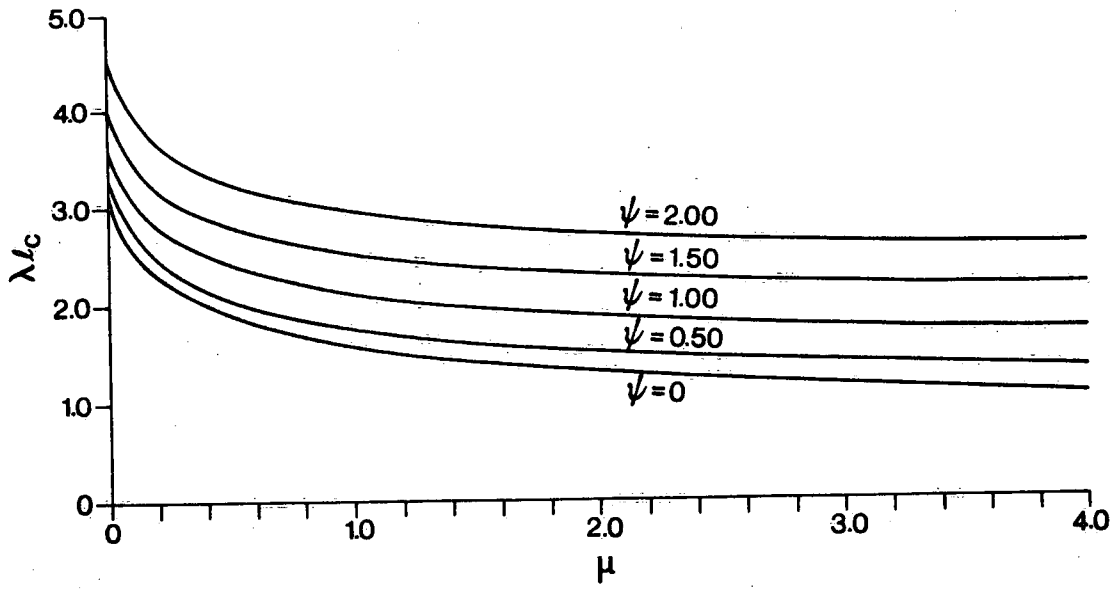

Fig. 9. Location of maximum bending moment for partly submerged ice sheet. Vertical bending case.

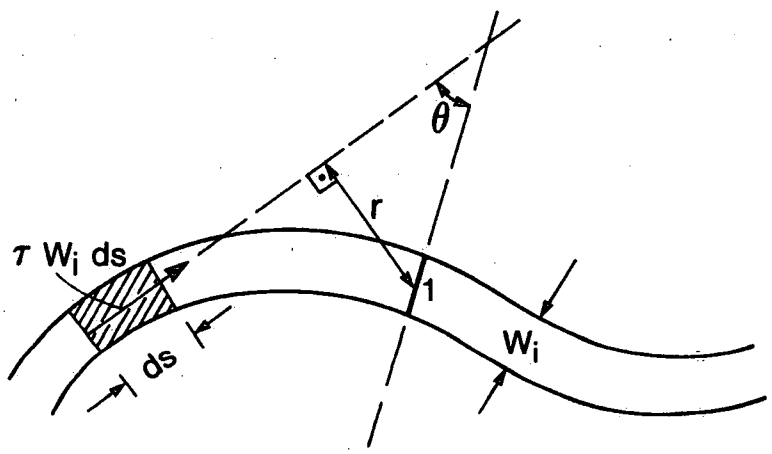

PLAN VIEW

Fig. 10. Generation of stresses at section 1 due to tangential force τ: shear = $(\tau W_i ds)\cos\theta$; axial force = $(\tau W_i ds)\sin\theta$; bending moment = $(\tau W_i ds)r$.

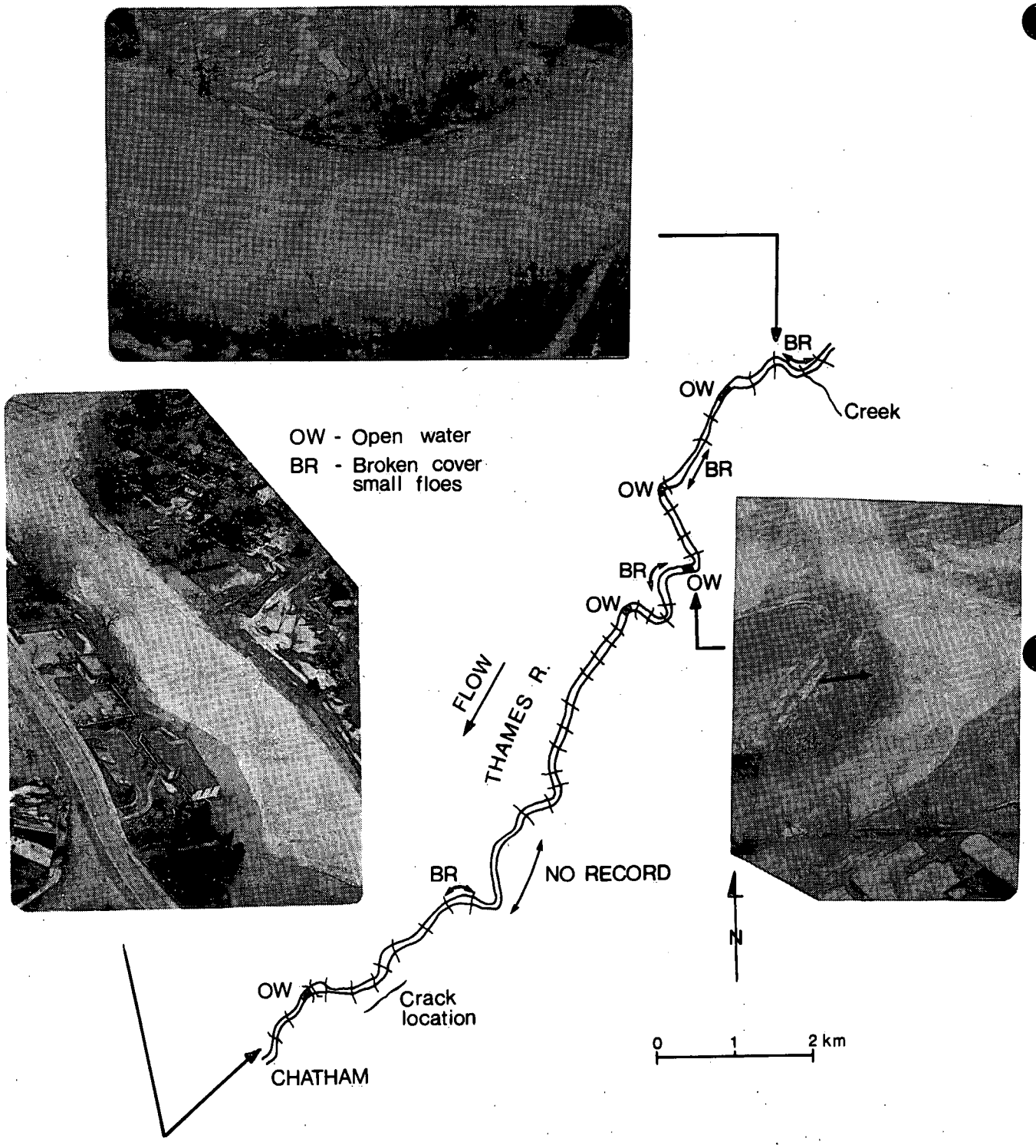

Fig. 11. Observed transverse crack pattern, Thames River above Chatham, Ontario, March 17, 1982.

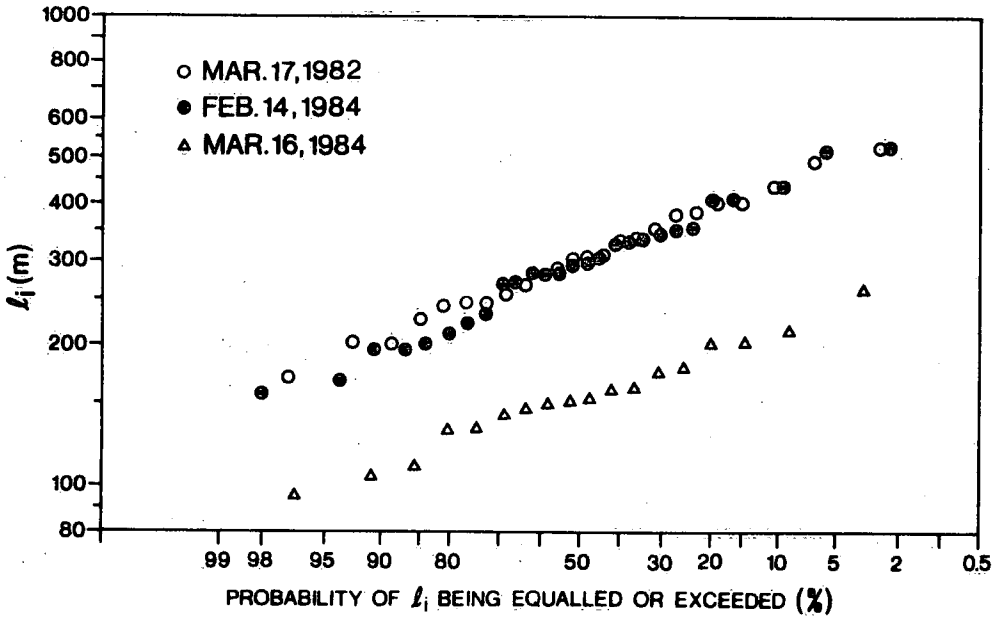

Fig. 12. Statistical distributions of lengths of ice sheets observed in the Thames River.

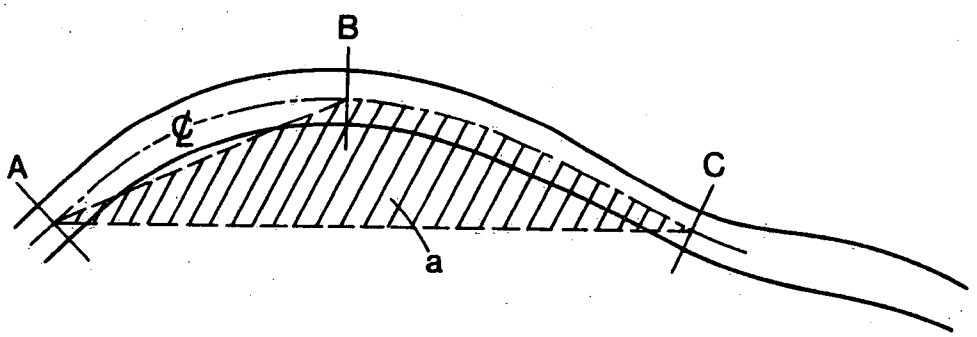

Fig. 13. Definition sketch for Equation 22; horizontal bending case.

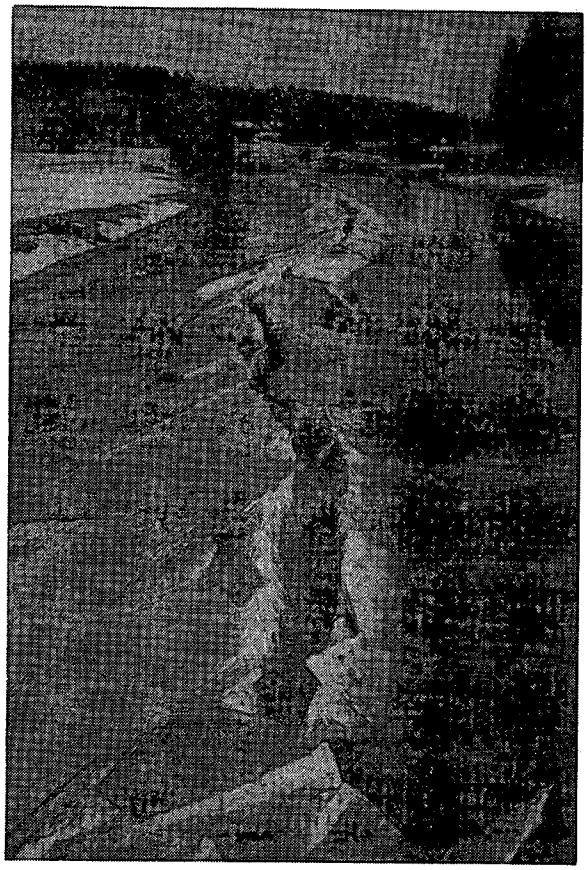

Fig. 14. Single longitudinal crack and uplifted strips due to rise in water level. Channel width ≈10m (courtesy E. Kuusisto).

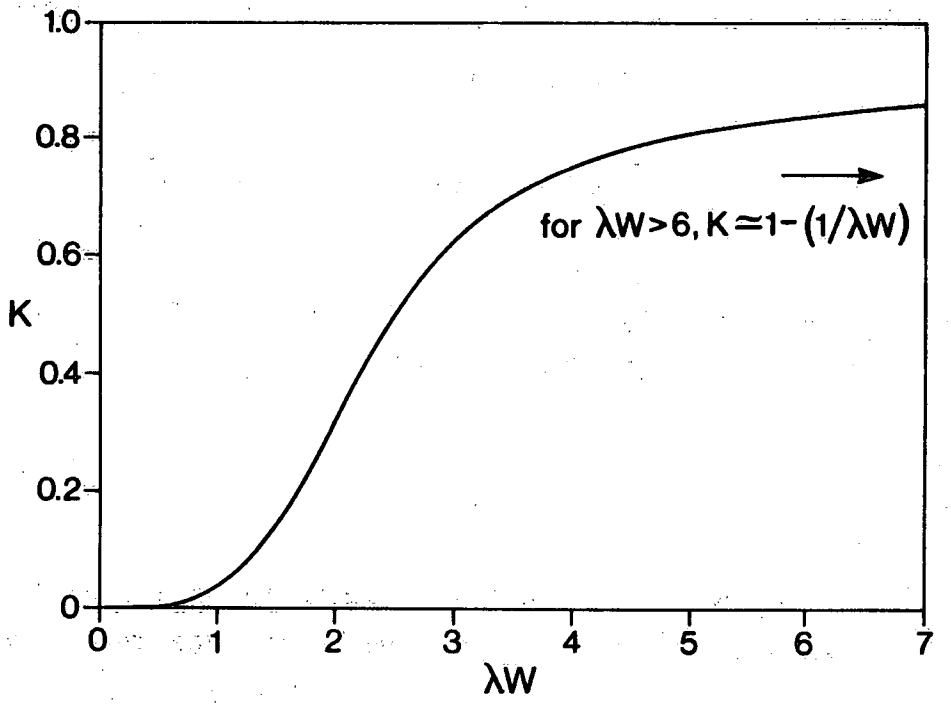

Fig. A.1. Variation of coefficient K with λW
(K = averaged ice deflection/uplift pressure head).

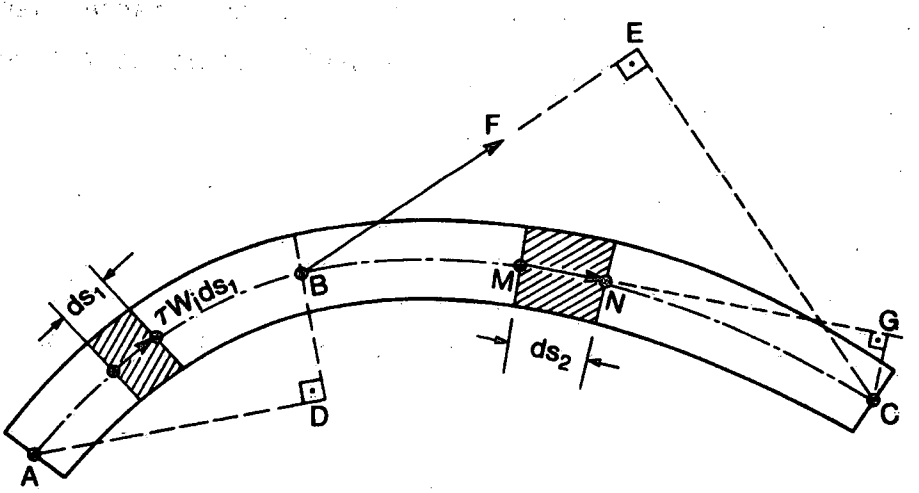

Fig. D.1. Sketch illustrating bending moments at point C.
Horizontal bending case.

APPENDIX A

Relationship of Uplift Pressure to Flow Characteristics

When the discharge begins to increase in the channel, the flow becomes unsteady. The continuity equation reads

$$\frac{\partial A}{\partial t} + \frac{\partial Q}{\partial x} = 0 \qquad (A.1)$$

in which A = flow area; Q = discharge; t = time; and x = longitudinal distance. Prior to crack formation, i.e., while the ice cover remains attached to the sides, the flow area is equal to $A_o + B_o \bar{w}$, with A_o, B_o = initial area and width respectively and $\bar{w}$ = average ice deflection. Hence, Eq. A.1 gives

$$\frac{\partial \bar{w}}{\partial t} = - \frac{\partial q}{\partial x} \qquad (A.2)$$

in which $q = Q/B_o$. For relatively short times and channel lengths, the unsteady flow could be assumed to approximately behave as a "frozen" wave form so that

$$\frac{\partial q}{\partial t} + C \frac{\partial q}{\partial x} = 0 \qquad (A.3)$$

in which C = celerity. Eq. A.3 may then be substituted in Eq. A.2 to obtain, after integration

$$\bar{w} = \Delta q/C \qquad (A.4)$$

in which $\Delta q = q - q_o$. Moreoever, the average ice deflection can be expressed as

$$\bar{w} = kp/\gamma \tag{A.5}$$

in which p = uplift pressure; γ = unit weight of water; and k = a coefficient that can be calculated by integration of ice deflections across the channel (see Fig. A.1). Substituting Eq. A.5 in Eq. A.4 gives

$$p = \frac{1}{k} \gamma \Delta q/C \tag{A.6}$$

As an example, consider the Thames River near Thamesville where typical values of h_i and W are 0.3 m and 40 m respectively. Using E = 1.4 GPa and σ_i = 600 kPa gives λW = 6.7, λh_i = 0.050 and p_f = uplift pressure for crack formation = 1.5 kPa. The value of C is about 1 m/s while Fig. A.1 indicates k = 0.85. Using Eq. A.6 gives $\Delta q \simeq 0.13$ m^2/s whereby the rise in discharge, required to form longitudinal cracks is 0.13 x 40 = 5.4 m^3/s which, at the site under consideration, occurs within 3 to 4 hours from the start of discharge rise. The longitudinal pressure gradient $\partial p/\partial x$ can be estimated using Eqs. A.6 and A.3, as

$$\frac{\partial p}{\partial x} = -\frac{\gamma}{kC^2} \frac{\partial q}{\partial t} \tag{A.7}$$

For the Thames River example, $\partial q/\partial t \simeq 10^{-5}$ m^2/s^2. Over a distance of (say) 100 m, the change in pressure is only 0.01 kPa which is negligible relative to p_f. Hence, the longitudinal variation of p is very small which jusitifies the use of the simple beam theory.

The effects of the vertical ice acceleration can be neglected, if (Billfalk 1982b)

$$4h_i \left| \frac{\partial^2 w}{\partial t^2} \right| \ll gw \tag{A.8}$$

Using Eq. A.4, Eq. A.8 can be recast as

$$\frac{4h_i}{g\Delta q}\left|\frac{\partial^2 q}{\partial t^2}\right| \ll 1 \qquad \text{(A.9)}$$

If $\partial^2 q/\partial t^2$ is approximated by $\Delta q/\Delta t^2$ with Δt = time elapsed since the start of runoff, Eq. A.9 can be re-written as

$$\frac{4h_i}{g\Delta t^2} \ll 1 \qquad \text{(A.10)}$$

For the Thames River example, h_i = 0.30 m so that Eq. A.10 is satisfied for Δt's exceeding 2s.

APPENDIX B

Conditions for Neglecting Vertical Ice Acceleration - Wave Breaking

Using data by Sorensen (1978), Billfalk (1982b) deduced that the vertical acceleration of the ice can be neglected, if

$$4\, h_i \left| \frac{\partial^2 w}{\partial t^2} \right| \ll gw \tag{B.1}$$

Assuming that during the short time interval for which an ice sheet is deformed and fractured by the incoming wave, the ice deflection form moves downstream without changing in shape and amplitude, we have

$$\frac{\partial w}{\partial t} \simeq - C \frac{\partial w}{\partial x} \tag{B.2}$$

in which C = celerity of the wave form. Hence

$$\frac{\partial^2 w}{\partial t^2} \simeq C^2 \frac{\partial^2 w}{\partial x^2} \tag{B.3}$$

Moreover, $\partial^2 w/\partial x^2 = M/EI$ so that Eq. B.1 may be recast as:

$$\frac{4 h_i C^2}{gEI} \quad \frac{|M|}{w} \ll 1 \tag{B.4}$$

It may now be noted that $|M|$ is limited by the flexural strength of the ice cover, i.e., $|M| \leq \frac{1}{6} \sigma_i h_i^2$. Noting also that $I = h_i^3/12$, Eq. B.4 becomes

$$\left(\frac{8\sigma_i}{E}\right) \frac{C^2}{gw} \ll 1 \tag{B.5}$$

For an order-of-magnitude estimate, Billfalk assumed that $w \simeq h_i$. Putting $\sigma_i \simeq 600$ kPa, $E = 6.8$ GPa and $C = 8$ m/s (one of the largest values observed during ice jam releases), the LHS of Eq. B.5 works out to 45 x $10^{-4}/h_i$ (h_i is in metres). For $h_i \simeq 0.5$ m, this becomes 0.01 which satisfies Eq. B.5 However, it can be shown that the value of w could be as little as 0.1 h_i at the locus of the maximum bending moment so that the LHS of Eq. B.5 would be about 0.1. This may still be considered negligible relative to 1.0, but, for wave celerities exceeding 8 m/s, Eq. B.5 may no longer be satisfied.

APPENDIX C

Bending of Ice Cover by Incoming Water Wave

Case 1. $l_0 = 0$

With reference to Fig. 6, we consider first the case $l_0 = 0$, i.e., an ice cover whose top surface is nowhere submerged. The load is:

$$q = q_0 e^{-\mu\lambda x} \tag{C.1}$$

in which

$$q_0 = \gamma\delta_0 \tag{C.2}$$

and δ_0 = rise of water surface above pre-wave value at the edge of the cover ($x = 0$); and x = distance downstream of the edge.

The ice cover is assumed to respond as a semi-infinite beam on an elastic foundation. The bending moment M is then (Hetenyi 1946):

$$M = \frac{\gamma w_0}{\lambda^2} F_3(\xi) + \frac{\gamma\theta_0}{\lambda^3} F_4(\xi) - \frac{1}{\lambda} G \tag{C.3}$$

in which

$$\xi = \lambda x \tag{C.4}$$

and w_0 = deflection at $x = 0$; θ_0 = ice slope at $x = 0$, i.e., $\theta_0 = (dw/dx)_0$. The functions F_3, F_4 and F_1, F_2 (not explicitly shown in Eq. C.3) are defined by:

$$F_1(\xi) = \text{Cosh}\xi \cos\xi \tag{C.5}$$

$$F_2(\xi) = \frac{1}{2}(\text{Cosh}\xi \sin\xi + \text{Sinh}\xi \cos\xi) \tag{C.6}$$

$$F_3(\xi) = \frac{1}{2}\text{Sinh}\xi \sin\xi \tag{C.7}$$

$$F_4(\xi) = \frac{1}{4}(\text{Cosh}\xi \sin\xi - \text{Sinh}\xi \cos\xi) \tag{C.8}$$

The following relationships apply (Hetenyi 1946):

$$\frac{dF_1}{d\xi} = -4F_4; \frac{dF_2}{d\xi} = F_1; \frac{dF_3}{d\xi} = F_2; \frac{dF_4}{d\xi} = F_3 \tag{C.9}$$

The quantity G in Eq. C.3 is given by:

$$G = \frac{1}{\lambda}\int_0^u q\,(u)\, F_2\,[\lambda(x-u)]du \tag{C.10}$$

in which u is a dummy variable and q is defined in Eq. C.1. Let:

$$\sigma = \lambda(x-u) \tag{C.11}$$

Then, Eq. C.10 can be manipulated to obtain

$$G = \frac{q_o e^{-\mu\xi}}{\lambda}\int_0^\xi e^{\mu\sigma} F_2(\sigma)\, d\sigma \tag{C.12}$$

Using Eqs. C.5 to C.9, Eq. C.12 can be further reduced to

$$G = \frac{4}{4+\mu^4}\frac{q_o}{\lambda}\{F_3 - \mu F_4 - \frac{1}{4}\mu^2(F_1 - e^{-\mu\xi}) + \frac{1}{4}\mu^3 F_2\} \tag{C.13}$$

Substituting Eq. C.13 in Eq. C.3 and re-arranging gives

$$M = aF_3 + bF_4 + c(F_1 - e^{-\mu\xi}) - dF_2 \tag{C.14}$$

in which

$$a = \frac{\gamma w_o}{\lambda^2} - \frac{4q_o}{\lambda^2(4+\mu^4)} \tag{C.15}$$

$$b = \frac{\gamma \theta_o}{\lambda^3} + \frac{4q_o\mu}{\lambda^2(4+\mu^4)} \tag{C.16}$$

$$c = \frac{\mu^2 q_o}{\lambda^2(4+\mu^4)} \tag{C.17}$$

$$d = \frac{\mu^3 q_o}{\lambda^2(4+\mu^4)} \tag{C.18}$$

Substituting Eqs. C.5 to C.8 and C.13 in Eq. C.3 and re-arranging, gives:

$$M = e^{\xi}\{\sin\xi\ (\frac{a}{4} + \frac{b}{8} - \frac{d}{4}) + \cos\xi(\frac{c}{2} - \frac{b}{8} - \frac{d}{4})\}$$

$$+ e^{-\xi}\{\sin\xi(\frac{b}{8} - \frac{a}{4} - \frac{d}{4}) + \cos\xi(\frac{b}{8} + \frac{c}{2} + \frac{d}{4})\}$$

$$- ce^{-\mu\xi} \tag{C.19}$$

Since we have assumed a semi-infinite beam, $M \to 0$ for $\xi \to \infty$, hence

$$\frac{a}{4} + \frac{b}{8} - \frac{d}{4} = 0 \tag{C.20}$$

$$\frac{c}{2} - \frac{b}{8} - \frac{d}{4} = 0 \tag{C.21}$$

Solving for a and b gives

$$a = 2(d-c) \tag{C.22}$$

$$b = 2(2c-d) \tag{C.23}$$

Using Eqs. C.15 to C.18 and C.22, C.23 gives after some algebra

$$w_o = \frac{2q_o}{\gamma} \frac{\mu + 1}{(\mu+1)^2 + 1} \qquad (C.24)$$

(which is the same as Eq. 18 of the main text)

$$\theta_o = \frac{2\lambda q_o}{\gamma} \frac{\mu}{(\mu+1)^2 + 1} \qquad (C.25)$$

$$M = \frac{\mu^2 q_o}{\lambda^2(4+\mu^4)} [e^{-\xi}\{(1-\mu)\sin\xi + \cos\xi\} - e^{-\mu\xi}] \qquad (.26)$$

which is the same as Eq. 17 of the main text).

To ensure that the top of the edge of the ice is not submerged we should have the condition

$$w_o + (1 - s_i)h_i \geq \delta_o \qquad (C.27)$$

(It may be noted via Eq. C.24 that the bottom of the edge of the ice cover is always submerged as should be the case in order for the analysis to be valid.)

Case 2, $l_o > 0$

With reference to Fig. 6, we denote the distance from the start of submergence by x, so that the edge of the cover is located at $x = -l_o$. The bending moment for $x \leq 0$ is:

$$M = \frac{-1}{2} q_s x'^2 \qquad (0 \leq x' \leq l_o) \qquad (C.28)$$

in which x' = distance downstream of the edge = $x + l_o$. At x = 0, the moment becomes

$$M_o = \frac{-q_s}{2\lambda^2}\psi^2 \tag{C.29}$$

in which

$$\psi = \lambda l_o \tag{C.30}$$

The bending moment in the region $x > 0$ is then (Hetenys 1946)

$$M = M_o F_1(\xi) + \frac{Q_o}{\lambda} F_2(\xi) + \frac{\gamma w_o}{\lambda^2} F_3(\xi) +$$

$$+ \frac{\gamma\theta_o}{\lambda^3} F_4(\xi) - \frac{1}{\lambda}\int_0^x q\, F_2[\lambda(x-u)]du \tag{C.31}$$

in which Q_o = shear force at $x = 0$. Proceeding as for the case $l_o = 0$, gives

$$M = aF_3 + bF_4 + c'(F_1 - e^{-\mu\xi}) - d'F_2 + M_o e^{-\mu\xi} \tag{C.32}$$

in which

$$c' = c + M_o \tag{C.33}$$

$$d' = d - \frac{Q_o}{\lambda} \tag{C.34}$$

Applying the condition $M = 0$ for $\xi \to \infty$, gives

$$a = 2(d' - c') \tag{C.35}$$

$$b = 2(2c' - d') \tag{C.36}$$

from which, after substitution of M_o and Q_o, we can obtain w_o and θ_o as (see also Eqs. C.15 to C.18):

$$w_o = 2\left\{\frac{q_o}{\gamma}\frac{\mu + 1}{(\mu+1)^2+1} + \frac{q_s}{\gamma}\psi\left(1 + \frac{\psi}{2}\right)\right\} \tag{C.37}$$

$$\theta_o = -2\lambda\{ \frac{q_o}{\gamma} \frac{\mu}{(\mu+1)^2+1} + \frac{q_s}{\gamma} \psi (1 + \psi)\} \quad (C.38)$$

Since the water surface intersects the top ice surface at x = 0, we have

$$w_o = \frac{q_o}{\gamma} - (1 - s_i) h_i \quad (C.39)$$

and, using Eq. C.37 and recalling tha $q_s = \gamma(1 - s_i)h_i$:

$$\frac{q_o}{q_s} = \frac{(\mu+1)^2 + 1}{\mu^2} (\psi + 1)^2 \quad (C.40)$$

which is identical to Eq. 15 of the main text. Eq. C.39 may also be re-cast as:

$$\frac{\gamma w_o}{q_s} = \frac{q_o}{q_s} - 1 \quad (C.41)$$

The ice deflection in the region x < 0 can be determined from:

$$EI \frac{d^2w}{dx'^2} = - M = \frac{q_s x'^2}{2} \quad (C.42)$$

Integrating once and noting that $\theta_o = (\frac{dw}{dx'})_{x'=l_o}$, gives

$$EI \frac{dw}{dx'} = EI\theta_o - \frac{1}{6} q_s l_o^3 + \frac{1}{6} q_s x'^3 \quad (C.43)$$

Integrating once more and noting that $w_o = (w)_{x'=l_o}$, gives the variation of w with x'.

The maximum ice deflection, w_e occurs at the edge of the cover and is given by

$$w_e = w_o - l_o\theta_o + \frac{q_s l_o^4}{8EI} \tag{C.44}$$

Substituting earlier findings and re-arranging:

$$\frac{\gamma w_e}{q_s} = \frac{\gamma w_o}{q_s} + 2\psi(\psi+1)\left(\frac{\psi+1}{\mu} + \psi\right) + \frac{\psi^4}{2} \tag{C.45}$$

which is the same as Eq. 16 of the main text.

With the above results, the bending moment becomes (Eq. C.32):

$$\frac{\lambda^2 M}{q_s} = e^{-\xi}\left[\alpha_1 \sin\xi + \alpha_2 \cos\xi\right] - \alpha_3 e^{-\mu\xi} \quad (x \geq 0) \tag{C.46}$$

in which

$$\alpha_1 = \frac{(1-\mu)(\psi+1)^2}{(\mu-1)^2+1} - \psi\left(1 + \frac{\psi}{2}\right) \tag{C.47}$$

$$\alpha_2 = \frac{(\psi+1)^2}{(\mu-1)^2+1} - \frac{\psi^2}{2} \tag{C.48}$$

$$\alpha_3 = \frac{(\psi+1)^2}{(\mu-1)^2+1} \tag{C.49}$$

Note that Eqs. C.46 to C.49 are identical to Eqs. 9 to 12 of the main text.

APPENDIX D

Bending on Horizontal Planes

Consider an ice sheet AB of width W_i, as sketched in Fig. D.1.. The force at an element ds_1 is equal to $\tau W_i ds$. The projections of this force on AD and BD are equal to the elementary normal and transverse forces exerted at B due to the element ds_1. The total force, F, at B due to ice sheet AB is then given by

$$F = \tau W_i (AB) \tag{D.1}$$

The bending moment caused by F at a point C, downstream of B is equal to F(CE). Taking into account Eq. D.1 shows that this moment, M_{AB}, is equal to $\tau W_i (AB)(CE)$ which, by inspection of Fig. D.1, gives:

$$M_{AB} = 2\tau W_i a_1 \tag{D.1}$$

in which a_1 = area of triangle ABC.

Considering next the bending moment at C due to an element ds_2 between points B and C, we have

$$dM_{BC} = \tau W_i ds_2 (CG) \tag{D.3}$$

But $ds_2(CG)$ is equal to twice the area of the elementary triangle CMN. Therefore

$$M_{BC} = 2 \tau W_i a_2 \tag{D.4}$$

in which a_2 is the area of the segment defined by the curve BMNC and the chord BC. The total moment is obtained by the sum of Eqs. D.2 and D.4 which results in Eq. 22 of the main text.